Bone 120 (2019) 393–402

Contents lists available at ScienceDirect

Bone

journal homepage: www.elsevier.com/locate/bone

Full Length Article

Spatially matching morphometric assessment of cartilage and subchondral bone in osteoarthritic human knee joint with micro-computed tomography

Birgitta Gatenholm[a,b], Carl Lindahl[c], Mats Brittberg[a,d], Vincent A. Stadelmann[e,f,*]

[a] Department of Orthopaedics, Institute of Clinical Sciences, The Sahlgrenska Academy at the University of Gothenburg, Gothenburg, Sweden
[b] Department of Orthopaedics, Sahlgrenska University Hospital, Mölndal, Sweden
[c] Department of Clinical Chemistry and Transfusion Medicine, Sahlgrenska University Hospital, Gothenburg, Sweden
[d] Region Halland Orthopaedics, Hallands Sjukhus, Kungsbacka, Sweden
[e] SCANCO Medical AG, Brüttisellen, Switzerland
[f] Department of Research and Development, Schulthess Klinik, Zürich, Switzerland

ARTICLE INFO

Keywords:
Osteoarthritic joint
Micro computed tomography
EPIC microCT
Cartilage lesion
Subchondral bone microarchitecture

ABSTRACT

Objective: The objective of this study was to develop a reproducible and semi-automatic method based on micro computed tomography (microCT) to analyze cartilage and bone morphology of human osteoarthritic knee joints in spatially matching regions of interest.

Materials and methods: Tibial plateaus from randomly selected patients with advanced osteoarthritis (OA) who underwent total knee arthroplasty surgery were microCT scanned once fresh and once after staining with Hexabrix. The articular surface was determined manually in the first scan. Total articular surface, defect surface and cartilage surface were computed by triangulation of the cartilage surface and the spatially corresponding subchondral bone regions were automatically generated and the standard cortical bone and trabecular bone morphometric indices were computed.

Results: The method to identify cartilage surface and defects was successfully validated against photographic examinations. The microCT measurements of the cartilage defect were also verified by conventional histopathology using safranin O–stained sections. Cartilage thickness and volume was significantly lower for OA condyle compared with healthy condyle. Bone fraction, bone tissue mineral density, cortical density and trabecular thickness differed significantly depending on the level of cartilage damage.

Conclusion: This new microCT imaging workflow can be used for reproducible quantitative evaluation of articular cartilage damage and the associated changes in subchondral bone morphology in osteoarthritic joints with a relatively high throughput compared to manual contouring. This methodology can be applied to gain better understanding of the OA disease progress in large cohorts.

1. Introduction

Osteoarthritis (OA) is the most common joint disease, causing morbidity and disability in patients worldwide [1–6]. In OA diagnostics the most widely used technique is still conventional x-ray [7–9]. There have been several studies, which aimed to develop OA diagnostics using radiography. However, conventional x-ray generally do not correlate well with patients experienced symptoms, are not sensitive enough to visualize early signs of changes in cartilage morphology and in essence are strictly 2-dimensional (2D) analysis [10,11]. A systematic review demonstrated that the relation of bone marrow lesions, synovitis and effusion to pain was moderate to strong. There was a weak or no relation of cartilage morphology or meniscal tears to pain. The relation of cartilage morphology to radiographic OA and radiographic joint space was found to be inconsistent [11].

Magnetic Resonance Imaging (MRI) offers several advantages as an imaging tool compared with radiography because it can visualize cartilage and its pathological changes without ionizing radiation. MRI is used in epidemiologic studies but much less in routine clinical setting, the main reason being high cost and sometimes long waiting time for MRI examination. The progress of OA can be followed using MRI with semi quantitative scoring approaches such as the Whole Organ MRI Score (WORMS), the Knee Osteoarthritis Scoring System (KOSS), Boston Leeds Osteoarthritis Knee Score (BLOCKS) and MRI Osteoarthritis Knee Score (MOAKS) [12,13]. A promising quantitative approach for diagnosing OA from MRI scans is trabecular bone texture

* Corresponding author at: Department of Research and Development, Schulthess Klinik, Lengghalde 2, 8004 Zürich, Switzerland.
E-mail address: vincent.stadelmann@kws.ch (V.A. Stadelmann).

https://doi.org/10.1016/j.bone.2018.12.003
Received 9 October 2018; Received in revised form 30 November 2018; Accepted 6 December 2018
Available online 08 December 2018
8756-3282/

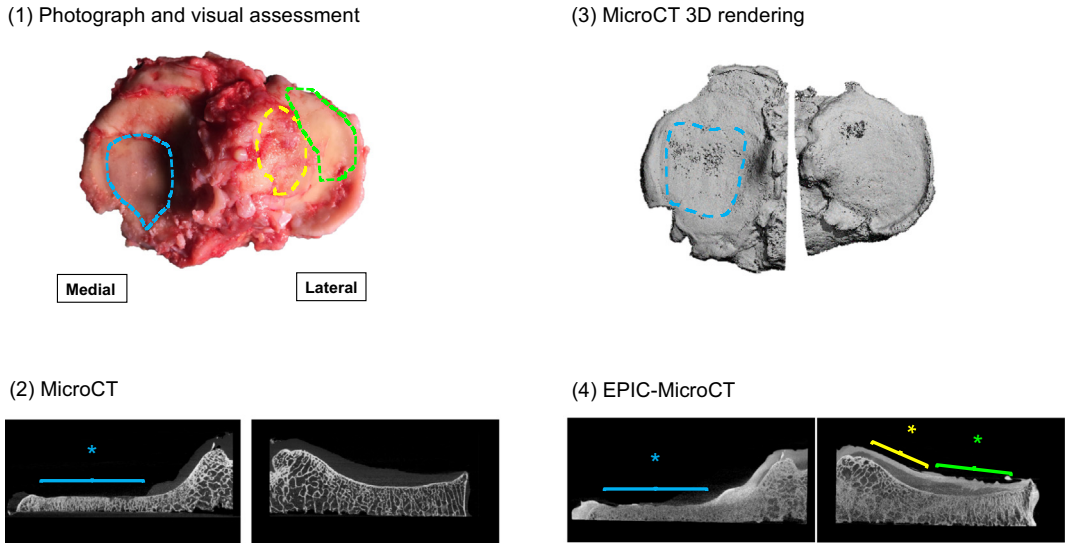

Fig. 1. (1) Photograph and visual assessment: immediately post-op the samples were photographed and evaluated visually by an expert. In this example, the medial condyle shows a large deep defect down to bone (blue), while cartilage of the lateral condyle has changing aspect between internal (yellow) and external (green) area, suggesting areas of healthier region and shallow cartilage defects. (2) The specimen is then microCT scanned. In the microCT scan the deep defect can be identified (blue star) but potential changes in the lateral cartilage cannot. (3) In a 3D rendering of the segmented scan the deep defect can be detected from excessive porosity on the condyle surface (blue dashed zone). (4) The specimen is finally EPIC-scanned. The defect can be observed (blue star) and variations in the Hexabrix staining can be observed in the lateral aspect (yellow and green stars), confirming visual assessment. Note that bone is blurred by the contrast agent infiltrations and cannot be analyzed in this scan. (For interpretation of the references to color in this figure legend, the reader is referred to the web version of this article.)

(TBT) analysis [14]. Texture analysis uses mathematical computations to increase the information obtainable from images [15]. Recently, subchondral TBT from MRI of tibia plateaus was significantly associated with histomorphometric outcomes. TBT analysis is therefore also a strong candidate to monitor the progression of OA in clinical studies; as confirmed by Mac Kay et al. recently [16,17].

OA was initially thought to be isolated to morphological changes in cartilage but is now considered a whole joint disease where the subchondral bone plays an important role in pain and disease development [18–23]. The subchondral bone is important for passive shock absorption in the joint and there is a vital interplay between the articular cartilage and subchondral bone [24]. Structural changes in the subchondral bone have an immediate effect on the overlying articular cartilage [18,25]. Studies with systematic mapping of the tibia plateau and the subchondral bone using micro computed tomography (microCT) in end stage OA from varying joint alignment showed significant condylar and intra condylar differences indicating that joint alignment has an effect on the microstructure of the subchondral bone plate [23,26].

There is an urgent need to develop technologies enabling visualization of early signs of OA and contributing to understanding of the sequence of morphological changes in joint. Promising results of imaging of cartilage microarchitecture using equilibrium partitioning of an ionic contrast agent (EPIC) in microCT were first reported in rodent models [27]. Negatively charged contrast agent molecules diffuse into the cartilage where glycosaminoglycan (GAG) depletion has occurred. After equilibrium is achieved the distribution of the ionic contrast agent is inversely related to the density of negatively charged GAGs. Sulphated glycosaminoglycans (sGAG) are structurally important in articular cartilage for maintaining its lubricant properties and loss of sGAG is an early sign of morphological changes in the articular cartilage related to OA [28].

MicroCT with ionic negatively charged contrast agent (EPIC microCT) is a promising but not yet fully explored technique for imaging GAG distribution in cartilage. Kokkonen et al. showed that there was a significant difference in penetration and x-ray attenuation of the contrast agent Hexabrix in healthy and mechanically damaged cartilage [29]. A recent study has also shown that quantitative contrast enhanced microCT can be used to assess the depth variation of GAG in ex vivo articular cartilage [30,31]. Research on animals have shown accurate measurement and cadaveric knee joint scanning using CT arthrography (CTa) have shown promising results [32–35]. CTa has also been introduced in vivo in clinical settings where a recent study showed a good correlation between CTa and sGAG measured using ex vivo EPIC microCT [36].

Our aims with the present study were to develop a methodology to evaluate morphology in spatially matching regions of cartilage and subchondral bone in OA patients using microCT and EPIC microCT. To the best of the authors´ knowledge, this has not been done previously, probably because while both methods use the same imaging device, the resulting images are different enough that one faces the challenges usually associated with multimodal imaging [37], such as co-registration and co-localization of regions of interest (ROI). In particular, in the OA context, one has to define spatially matching ROIs in the articular surface and the subchondral bone in order to study their interactions. In “traditional” microCT image processing, ROIs are drawn manually in axial or sagittal slices, which for articular cartilage, is tedious and imprecise because cartilage has similar x-ray absorption to neighboring tissues and is not in a single plane.

To overcome this difficulty, we present a semi-automatic workflow to analyze tibia condyles with automatic ROI generation, defects identification, and damage mapping.

2. Materials and methods

2.1. Sample selection

Twelve tibia plateaus were retrieved from patients with advanced OA who underwent total knee arthroplasty surgery at Sahlgrenska University Hospital, Sweden following a procedure approved by the Ethical committee in Gothenburg, Sweden and informed consent was not required. The tibia plateaus where retrieved during surgery and stored in phosphate buffer saline (PBS, Sigma Aldrich) prior to analysis. To prevent cartilage degeneration, the PBS used throughout this study contained protease inhibitors (1% Protease Inhibitor Cocktail Set I, CalBiochem, San Diego, CA). Three plateaus split into six condyles were

used to determine the dynamics of contrast agent Hexabrix staining in human knee cartilage.

2.2. Macroscopic observations

Directly post-operatively, the samples were photographed (Fig. 1), and split into medial and lateral condyles through the eminentia tibia (to fit into a Ø7 cm microCT sample holder). The bone was washed multiple times with PBS and stripped of soft tissue such as rests of ACL and meniscus. An experienced surgeon visually inspected the specimens and cartilage defects were contoured on the photos. The annotated photos were imported into Fiji [38] where the total condyle surface (Cond.S) and defect surface (Def.S) were extracted using measuring tools, and Defect surface fraction (Def.S/Cond.S) was computed (see Fig. 1).

2.3. MicroCT analysis

2.3.1. Baseline microCT

After removal of excess fluid, the condyles were wrapped in cling-film and scanned in air with a cabinet cone-beam microCT scanner (μCT100 Scanco Medical, Bruttisellen, Switzerland) operated at 70 kVp, 200 uA, 500 ms; 1000 projections/180°. The slices were reconstructed across an image matrix size of 2048 × 2048 voxels, with a nominal voxel size of 36 μm, resulting in a scan volume 20 mm long and 75.3 × 75.3 mm in the axial plane (scan time 40 min).

2.3.2. EPIC microCT

After the baseline scan, the specimens were immersed in a solution of 40% ionic CT contrast agent Hexabrix (Hexabrix 320, Guerbet AG, Zürich CH) and 60% PBS at room temperature under slow agitation. First, six condyles were immersed for 4, 8, 16, 24 and 33 h and then re-scanned after each period to determine the diffusion dynamics of the contrast agent. It was determined that 20 h was an optimal staining time. All the following specimens were immersed in the solution once for 20 h and scanned. The second scan, referred to as “EPIC- scan” in reference to Palmer et al. [27], was performed with the same settings as the baseline scan. Finally, three specimens were immersed in PBS for 48 h after EPIC-scan to desorb Hexabrix before histological processing.

2.4. Image processing

The image processing algorithms were developed with EasyIPL, a high-level library of macros using the scanner softwares (SCANCO Image Processing Language, IPL and HP OpenVMS Digital Command Language, DCL).

2.4.1. Alignment and segmentation

The specimens were scanned with the cut surface flat on the holder's bottom. The scan data was first re-oriented to work in the sagittal plane, with medial and lateral condyle oriented left and right on the screen respectively to facilitate image interpretation. Trabecular, cortical bone and cartilage were segmented from the baseline scans based on their specific x-ray absorptions and morphometry as described in Fig. 2.

2.4.2. ROIs definition

Multiple ROIs were defined: articular surface, cartilage, cartilage defect, exposed bone, trabecular and cortical bone.

First, the articular surface was identified: each scan was Gaussian-filtered ($\sigma = 0.5$, support = 1) to reduce noise, bone segmented (threshold = 280mgHA/ccm) and the articular surface was identified visually in 3D rendering. The contour of the articular surface was drawn on an axial projection. Bone surface was then generated by closing the segmented bone (d = 20 voxels) and finally, the articular surface contour was projected onto bone surface to obtain the articular surface ROI (Fig. 3).

Cartilage defect was defined as the articular surface not covered by cartilage. To generate the defect ROI, bone surface was offset by two voxels in the Y direction and intersected with the cartilage object to create the articular surface with cartilage object; the articular surface with cartilage was masked off from the articular surface object to generate the cartilage defect ROI.

2.4.3. ROI projections to create sub-ROIs

The articular surface ROI and *articular surface defect* ROI were projected in the axial direction and intersected with cartilage, trabecular and cortical bone (using methods as above) to define the sub-ROIs, namely sub-cartilage/sub-defect trabecular bone, sub-cartilage/sub-defect cortical bone, and articular cartilage (Fig. 4 and Table 1).

2.4.4. Morphometric measurements

The total articular surface (AS.S), defect surface (D.S) and cartilage surface (C·S) were computed by triangulation of the object surface using a marching-cubes algorithm [39]. The standard cortical bone and trabecular bone morphometric indices were computed using voxel counting (BV/TV) and sphere fitting (Ct.Th, Tb.Th, Tb.Sp, etc.) [40].

2.4.5. Alignment of EPIC scans to baseline scans

The EPIC scans were aligned in space to the baseline scans, so that the ROIs defined at baseline could be used in the EPIC space directly. For this, bone was roughly contoured in the EPIC scans and it was used to register the scan to baseline scan using rigid registration, with a minimum correlation coefficient of 0.8, convergence criterion of 1×10^{-5}, and maximum 2000 iterations [41]. The ROIs defined in the baseline scan could then be reported to the EPIC scan using the inverse registration matrix. The cartilage sGAG content was estimated from the contrast agent concentration [27]. Staining intensity distribution was evaluated within articular cartilage by generating a histogram of the voxels' intensity (in HU) within the cartilage ROI. Cartilage stained fraction (normal vs low sGAG content) was evaluated by segmenting the image ($\sigma = 2$, support = 4, threshold = 4000 HU).

2.5. Histology

Tibia plateaus were sent to HistoCenter AB, Sweden for histology. The following protocol was used to treat the samples. (1) Decalcification: 12.5% EDTA, Sigma E5134, dissolved in deionized water over the intended period. (2) Dehydration: Isopropanol (Histolab 02150), in increasing concentrations from 90% to 100%, final steps in isopropanol occurred in 60 °C oven and samples were then mounted in paraffin. (3) Cutting: 5 μm thick slices. (4) Staining: Safranin-O, which was dissolved in distilled water. The order of the different components of the color method: Weigert HTX, Salty liquor, Fast Green, 1% Acetic acid, Safranin, then dehydration in 96%, 100% etOH and Xylene → assembly.

2.6. Validation of microCT with histology

The microCT slices corresponding to histological slices were manually determined in 3D, based on anatomical and feature landmarks. The total cartilage thickness and stained cartilage thickness were measured in Fiji along various vertical lines in histology and microCT slices. The stained thickness fraction was computed.

2.7. Statistical analysis

Data is expressed as Mean ± SD unless stated otherwise. The correlation between surface fraction from photographic examination and microCT analysis was evaluated by fitting a linear model with the *lm* function. Staining dynamics: a sigmoid function was fitted using Nonlinear Least Squares. Morphometric analysis: one-way ANOVA were performed using the aov function. Confidence levels $p < 0.05$ and

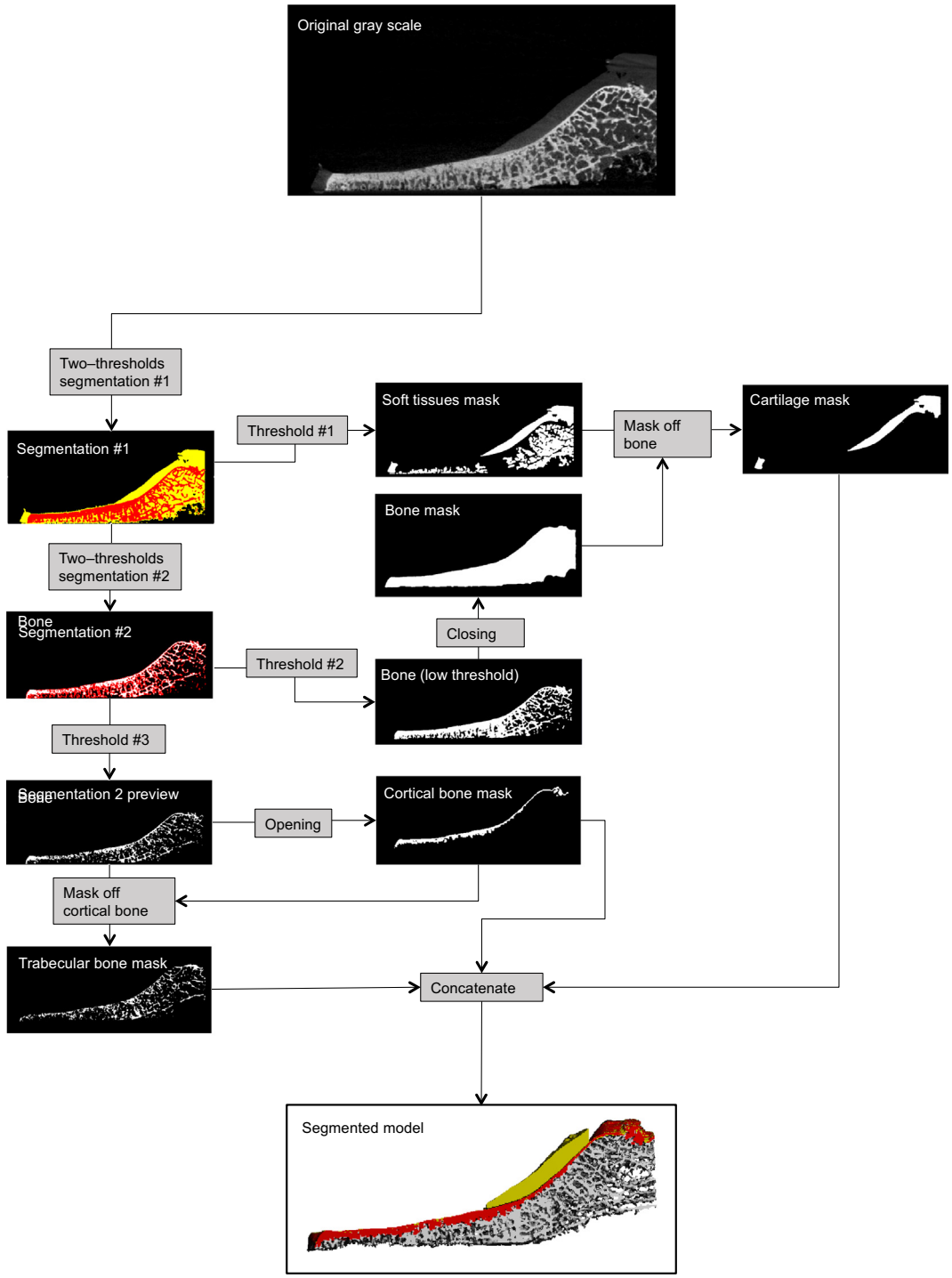

Fig. 2. Workflow diagram for segmentation of cartilage, cortical and trabecular bone. The grayscale image was smoothed with a Gaussian filter to reduce noise, and then segmented using three thresholds (σ = 1, support = 2, T = −300 HU for soft tissues; σ = 1, support = 2, T = 280 mgHA/ccm for trabecular bone; and σ = 0.5, support = 1, T = 480 mgHA/ccm for dense bone). The thresholds values were first estimated from the histograms in representative specimens and then visually refined by direct visual comparison of grayscale and segmented images slice by slice [23]. The segmented soft tissue and trabecular bone objects were cleaned of noise by an opening of two voxels. Trabecular bone was excluded from the dense bone object by an opening of 1 voxel followed by a component labeling to remove objects of < 500 voxels. The object was then closed by one voxel to create the cortical mask. The trabecular bone object was masked off of the cortical mask to generate the trabecular mask.

$p < 0.01$ were considered statistically significant and highly significant respectively. All analyses were performed in the R programming language (version 3.3.3) [42].

3. Results

3.1. Comparison of EPIC method with histology

Histology slices were obtained for three condyles and the corresponding microCT slices were manually determined. Safranin O stains

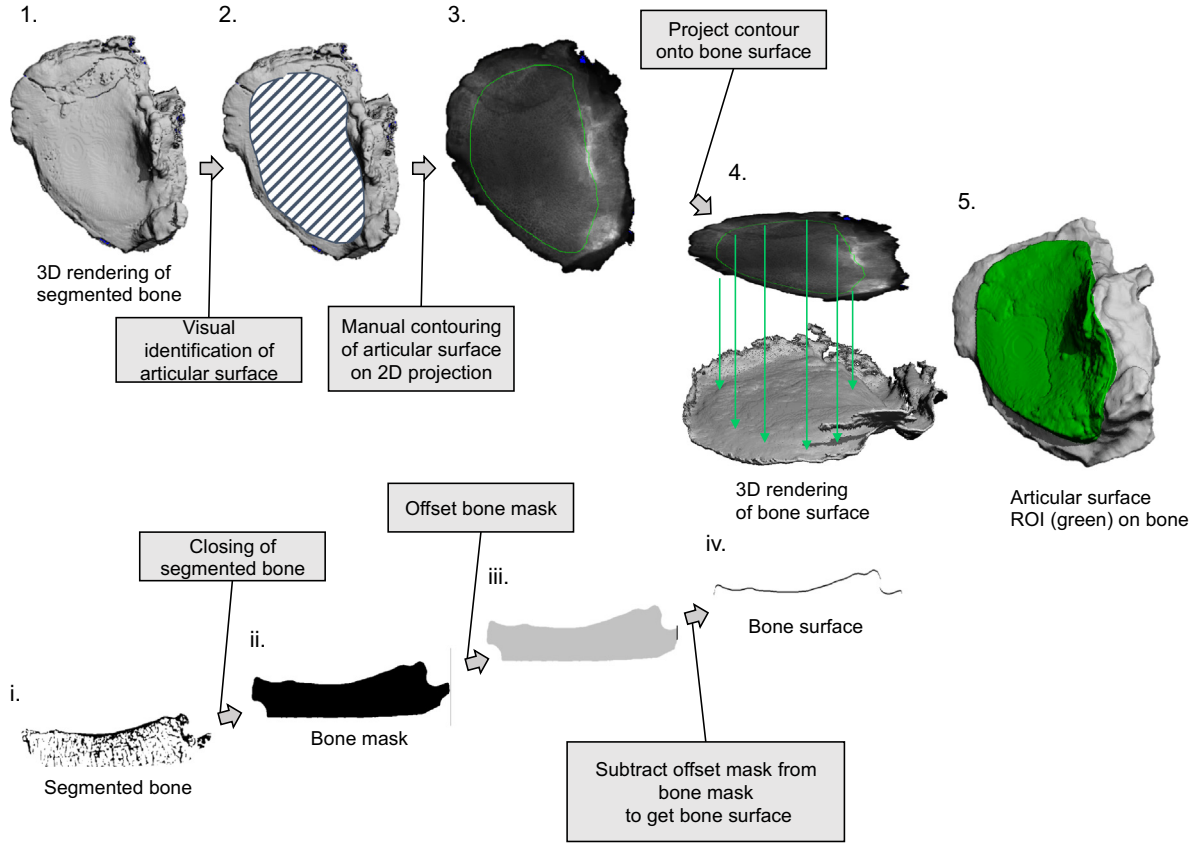

Fig. 3. Workflow diagram showing the definition of articular surface ROI by projection of a 2D contour onto bone surface. (1) Bone was rendered in 3D; (2) the articular surface was identified and (3) it was contoured on a 2D projection of the condyle. To generate bone surface, (i) bone was segmented, (ii) closed (d = 20 voxels) and (iii) offset by two voxels in Y and (iv) subtracted. (4) The articular surface contour was projected onto the bone surface to obtain (5) the articular surface ROI.

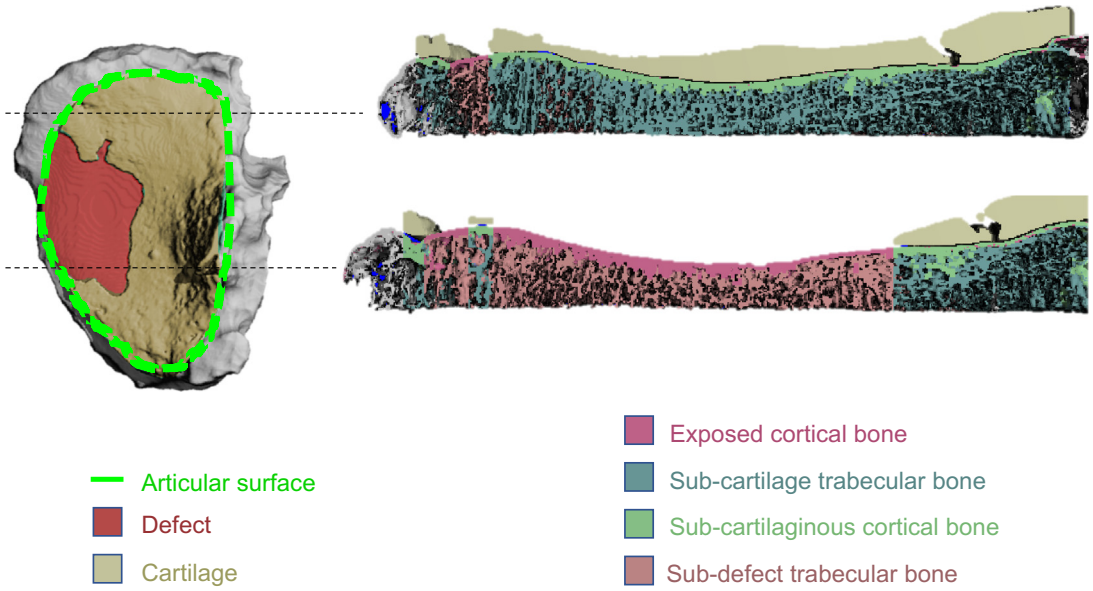

Fig. 4. Illustration of the various ROIs of the model. Articular surface, in dashed green is manually defined. Cartilage and defect ROIs are generated automatically and projected into bone to generate the bone sub-ROIs. (For interpretation of the references to color in this figure legend, the reader is referred to the web version of this article.)

red proportionally to sGAG content. Unhealthy cartilage shows only small areas with sGAG staining (red) indicating low amounts of proteoglycans, (Fig. 5B). In contrast histology slice of the healthier lateral condyle shows a large area with red staining sGAG (red) indicating high amounts of proteoglycans, (Fig. 5A). Subsequently, we could notice a progressive loss of glycosaminoglycans (sGAG content, red staining) in unhealthy cartilage. Finally, Fig. 5C shows a cartilage defect, down to subchondral bone. Fig. 5A–C also illustrates a qualitatively good match

Table 1
List of ROIs used, description and rationales.

ROI name	Description	Rationale/Usage
Articular surface	The manually drawn articular surface	All following ROIs are limited to this ROI in X and Y
Subchondral bone	Bone below the articular cartilage	Osteoarthritis is also a bone disease
Cartilage	Existing cartilage within articular surface	This ROI is also used in the registered EPIC scan
Sub-cartilage cortical bone	Cortical bone below existing cartilage	Exposed bone can be grinded by the joint movement
Sub-cartilage trabecular bone	Trabecular bone below existing cartilage	Subject to higher load
Defect	Surface of bone within articular surface but not covered by cartilage	The defect size shows the advance of the disease
Sub-defect cortical bone	Cortical bone below defect	Thickening of this bone may be a sign of early OA
Sub-defect trabecular bone	Trabecular bone below defect	Bone "protected" by cartilage is subject to less load

between microCT and histology.

3.2. Staining dynamics

Staining followed a sigmoid curve and reached a plateau around 18-20 h (Fig. 5D). The data was fitted with a sigmoid function (plain line) $A = a\ (1 - b\ e^{-t/c})$, where A = absorption; t = time; a, b, c are numerical parameters (best fit: $a = 3.03\,cm^{-1}$, b = 0.76, c = 7.09 h) in good agreement with the original findings from Palmer et al. [27].

3.3. Validations

Defect surface fraction from photographic examination vs microCT analysis correlated significantly with microCT defect fraction ($r^2 = 0.83$, $p < 0.001$). Similarly, the cartilage thickness fraction in histology correlated significantly with cartilage stained fraction measured with EPIC microCT ($r^2 = 0.83$, $p < 0.011$) (Fig. 6A).

3.4. Bone morphometry

Bone was categorized in three sub-regions: bone under intact cartilage (condyles without defect), bone under damaged cartilage (condyle with a full depth defect) and exposed bone under full-depth defect. Bone fraction (BV/TV), Trabecular thickness (Tb.Th), Tissue Mineral Density (TMD), Cortical Mineral Tissue Density (Ct.TMD) and Trabecular Tissue Mineral Density (Tb.TMD) were significantly affected by overlying cartilage status ($p < 0.05$); but cortical thickness (Ct.Th) was not (Fig. 6B).

3.5. Cartilage morphometry

In total, 23 condyles were analyzed; 13 had a cartilage defect down to bone and 10 were without a defect. Twelve of the defects (92%) were found in the medial condyle and one in the lateral condyle. The distribution of defect surface (in % of condyle surface) was bimodal with 60% of the condyles showing only small defects (< 20% of total condyle surface) and 30% showing large defects (> 35%). Cartilage thickness was significantly higher in intact condyles ($p = 0.029$). Hexabrix absorption seemed lower in intact condyles, but the difference was not statistically significant (Fig. 7A). Fig. 7B illustrates the distribution of cartilage thickness over all analyzed condyles.

4. Discussion

With an increasing incidence of OA there is today an urgent need for imaging techniques capable of capturing morphological changes of the cartilage and the subchondral bone as a whole. This should enable a better understanding of the cross talk between bone and cartilage during the progression of the disease. This study presents a new methodology for generating spatially matching ROIs in cartilage and bone. The methodology was applied to the medial and lateral tibia condyles of 12 patients with end-stage knee OA and varus joint alignment. A complete mapping of the cartilage surface and the microstructure of the underlying bone was obtained by combining native microCT scans and scans after immersing the samples in a solution of ionic CT contrast agent Hexabrix 320. The optimal staining time was determined to be 20 h to obtain an equilibrium and optimal visualization of the cartilage and by that the GAG content which negatively correlates with Hexabrix content [36]. Medial condyles with excessive damage were compared to lateral condyles with healthier cartilage and less or no macroscopically visual cartilage injuries. Significant difference ($p < 0.05$) was found in the condyles when comparing regions of bone under intact cartilage, bone under damage cartilage without full depth defect and exposed bone under defect in the morphometric measurements of bone fraction, bone tissue mineral density, cortical bone tissue mineral density and trabecular thickness. Subchondral bone changes and trabecular bone loss as early post-traumatic OA signs have been seen in earlier studies with in vivo HR-pQCT scans of patients who underwent ACL reconstruction [43,44].

The accuracy of EPIC microCT images of the cartilage health were verified by conventional histopathology using safranin O–stained sections. Previous studies have shown a good correlation between histopathological findings and images created using contrast enhanced microCT where pathological changes in articular cartilage and subchondral bone were clearly visualized [45]. Similarly we saw in our study a significant positive correlation between the cartilage thickness fraction measured in histology compared to the one measured with EPIC microCT.

Defining ROIs in articular cartilage surface manually, and in particular of cartilage defects, is often excessively simplified, for example van Tiel et al. used rectangular ROIs [36], otherwise it becomes overly time consuming or imprecise. To overcome this limitation, we developed a semi-automatic method for ROI generation where, after the articular surface is identified and contoured in a single image, it is automatically projected onto the subchondral bone and all eight sub-ROIs are generated. The precision of the automatic defect detection in microCT images was validated against analysis of post-operative photographs. Correlation between microCT and photographic defect surface was very good, despite variations in photographic measurements that may come from the convex surface of the plateaus.

Early onset of cartilage degradation is seen in young patients developing post-traumatic OA after ligament tears such as ACL injury. Evidence suggests that subchondral bone changes and oedema play a pivotal role in disease development and can be observed even prior to development of degradation in the articular cartilage. A recent study examining the subchondral bone plate and cartilage thickness with MRI and HR-pQCT [44] in young female patients with ACL reconstructed knees showed significant thickening of the subchondral bone plate in areas where significant differences in cartilage thickness were not detected [46,47]. Using the automatically generated ROIs in our sample of tibial plateaus, spatial variations in bone morphometry could be significantly associated with spatial variations of OA stages. Subchondral bone morphometry under apparently intact cartilage differed significantly between condyle with defects and condyles without defects, suggesting that morphometric changes occurred already before cartilage defects reach full-depth.

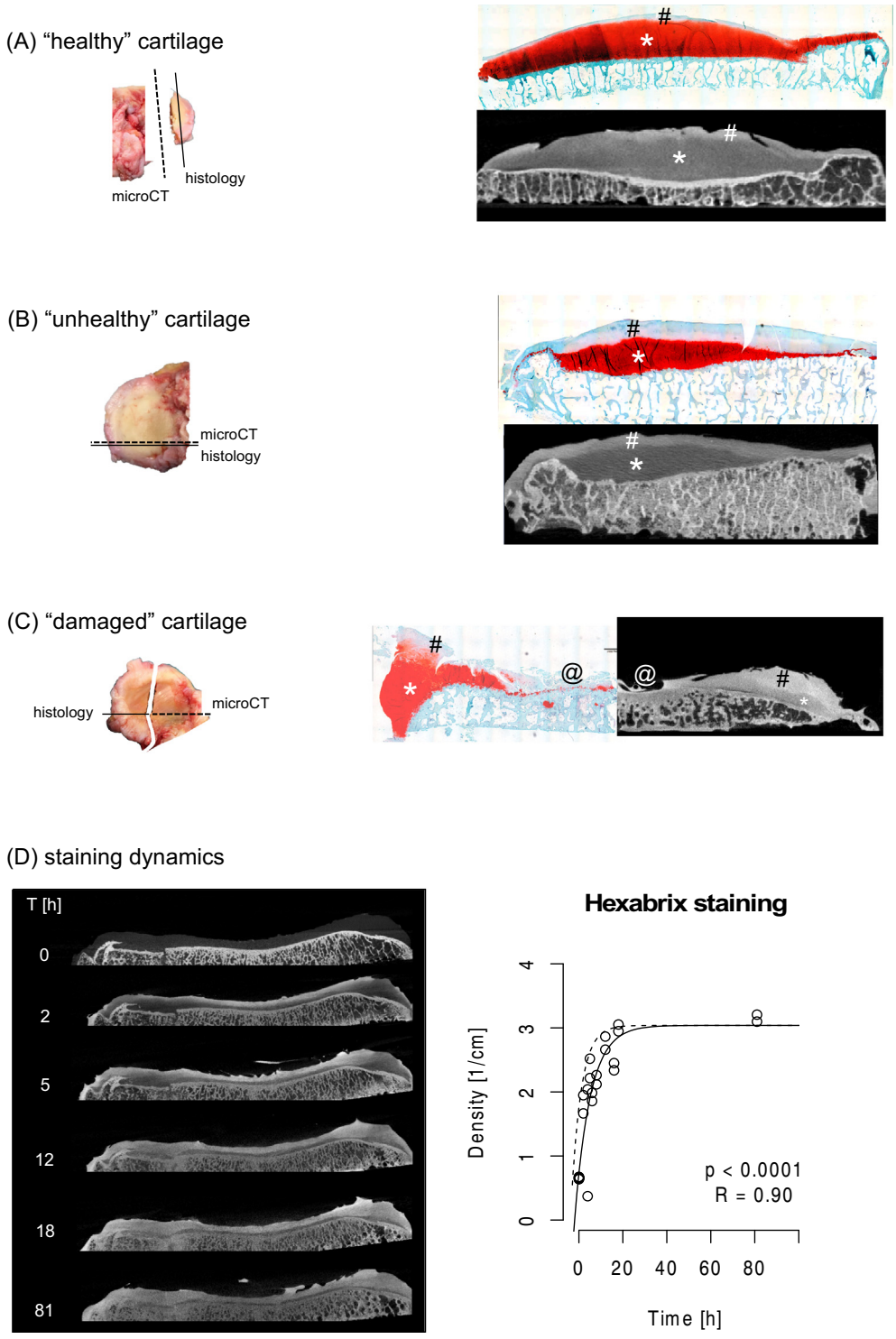

Fig. 5. (A–C) Comparison between histology and EPIC microCT: (A) A “healthy” condyle was separated in two parts after surgery, one part was used for EPIC microCT, one was used for histology (Safranin-O). (B) A condyle was first EPIC-scanned then desorbed and used for histology. (C) like (A) in two pieces. * shows healthy cartilage with high sGAG content and # low sGAG content and @ shows defect. Note the qualitatively good match between histology and microCT. (D) Results of the staining dynamics study. (Left) shows evolution of staining in grayscale EPIC scans over the course of 81 h of staining. (Right) The data was fitted with a sigmoid function (plain line). The dashed line shows original findings from Palmer et al. [27].

Finally, it was recently shown that cartilage at the posterior aspect of the medial condyle may be frequently (89%) preserved in advanced grades of OA [48]. Accordingly, we categorized the position of the defect in ten unfragmented specimens with defects, as anterior, centered or posterior, based on the center of the defect relative to the center of the condyle. Five defects were centered; four were anterior and only one posterior (90% of posterior cartilage was preserved).

Our study had several limitations. First of all, only 12 patients, all with medial OA were examined since the main aim was to test and validate the new imaging methodology. The low number of specimens used and the homogeneity of the specimens (all varus knee end stage OA) makes it hard to draw any wide conclusions for the whole OA population, especially for early stage OA. Second, depending on how advanced the OA was, there were variations in the tibial surgical cutting which lead to a variation in specimen thickness. This may not affect the analysis of cartilage but affects the thickness of the subchondral bone analyzed. Third, the articular surface was manually drawn and sometimes on fragmented specimens somewhat hard to define. The manual drawing gives room for some imperfection when it comes to specimens damaged during surgery.

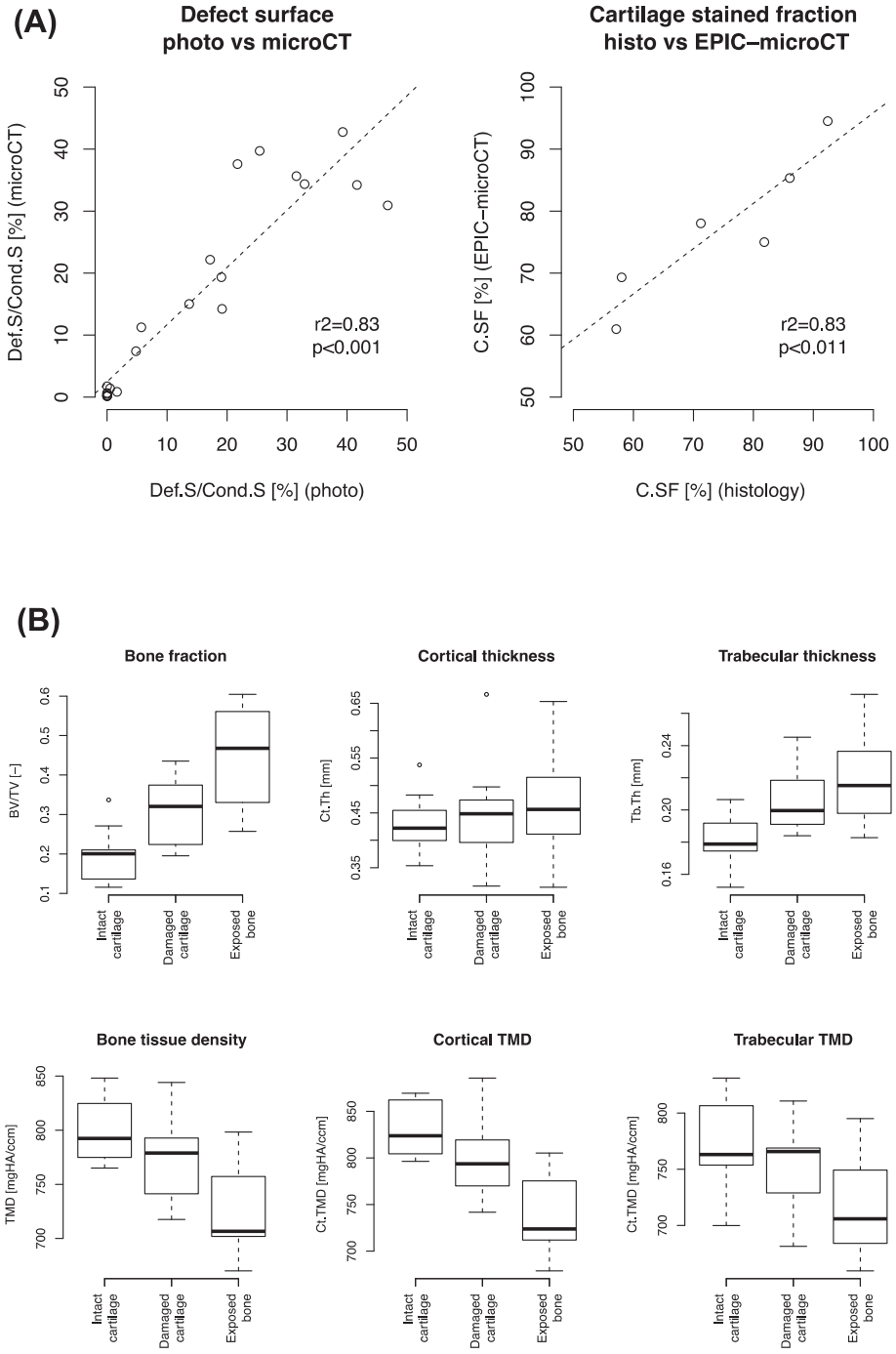

Fig. 6. (A Left) shows the correlation between the defect surface evaluated by microCT and the same evaluated from photographic analysis. (A Right) shows the correlation between the cartilage stained fraction (C.SF, calculated as stained thickness/cartilage thickness) from microCT and histological data. (B) Bone morphometric results in function of overlying cartilage status: BV/TV, Tb.Th, TMD, Ct.TMD and Tb.TMD were significantly affected by overlying cartilage status ($p < 0.0001$, $p = 0.0012$, $p = 0.0007$, $p < 0.0001$, $p = 0.0193$ respectively), but not Ct.Th ($p = 0.6473$).

5. Conclusion

In conclusion, this study introduces and illustrates a new workflow for the analysis of microCT scans of human knee joints, in which spatially matching ROIs are semi-automatically generated in cartilage and subchondral bone, based on cartilage damage. The workflow can be used to correlate spatially the degree of OA damage to subchondral bone quality. In the future, this workflow could be ported to in vivo HRpQCT or MRI scans analysis to identify early changes in the subchondral bone morphology prior to OA development, and could hopefully help establish biomarkers for the detection of early degradational changes, especially in young patients for whom there are many more joint preservation treatment alternatives before a total knee arthroplasty.

Acknowledgements

We would like to thank the Orthopaedic Surgents at the Orthopaedic department, Arthroplasty unit at Sahlgrenska University Hospital, Gothenburg, Sweden who provided patients and assistance in

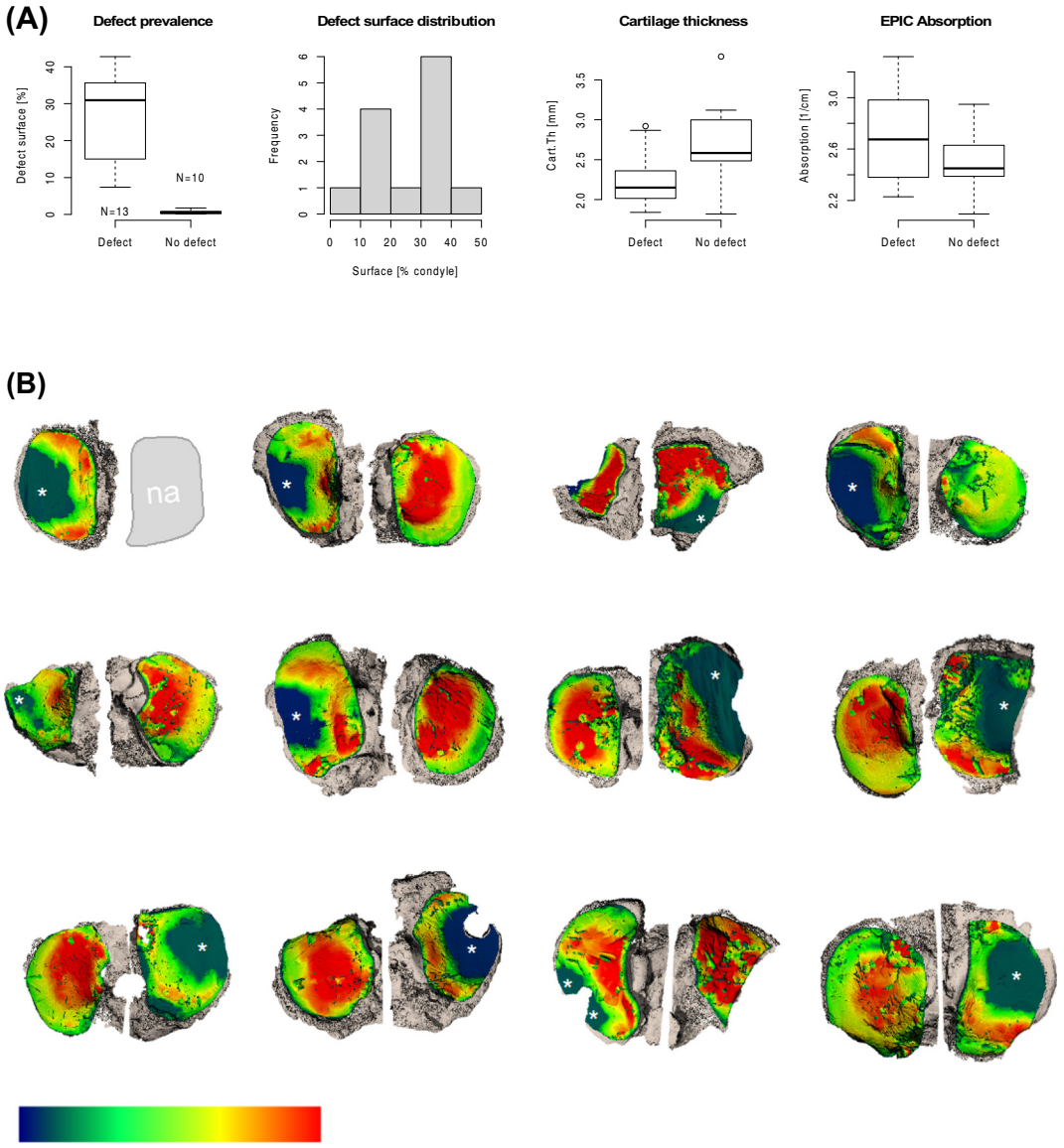

Fig. 7. (A) Defect prevalence: 13 condyles had full depth cartilage defects and 10 were intact. Defect surface distribution was bimodal. Cartilage thickness was statistically lower in condyles with full depth defect ($p = 0.029$) but EPIC absorption was not. (B) Overview of cartilage thickness for all 23 tibia plateaus condyles. Twelve full-depth defects (*) were located on the medial condyle and only one on the lateral condyle.

tissue sampling; Camilla Brantsing at the Department of Clinical Chemistry and Transfusion Medicine, Sahlgrenska University Hospital, Gothenburg, Sweden for microscopic imaging of histology sections; Guerbet AG, Zürich who generously provided Hexabrix; and finally Markus Burkhart of SCANCO Medical who helped with staining of the specimens.

Author contributions

BG, MB and VS designed the study. BG, CL and VS performed the experimental work. VS performed the micro CT analysis, created the algorithms and analyzed the data. BG, CL, MB and VS critically evaluated the study. BG, CL and VS drafted the manuscript. MB VS and BG reviewed and finalized the article. All authors discussed on the work and gave final approval.

Ethics approval

Tissue sampling was approved by patients and followed a procedure approved by the Ethics Committee at University of Gothenburg. Since tissue samples were de-identified, the need for an ethical approval was waived.

Conflict of interest

BG, CL, MB and VS have no conflict of interest to declare.

References

[1] M. Cross, E. Smith, D. Hoy, S. Nolte, I. Ackerman, M. Fransen, L. Bridgett, S. Williams, F. Guillemin, C.L. Hill, L.L. Laslett, G. Jones, F. Cicuttini, R. Osborne, T. Vos, R. Buchbinder, A. Woolf, L. March, The global burden of hip and knee osteoarthritis: estimates from the Global Burden of Disease 2010 study, Ann. Rheum. Dis. 73 (2014) 1323–1330, https://doi.org/10.1136/annrheumdis-2013-204763.

[2] H. Kotlarz, C.L. Gunnarsson, H. Fang, J.A. Rizzo, Insurer and out-of-pocket costs of osteoarthritis in the US: evidence from national survey data, Arthritis Rheum. 60 (2009) 3546–3553, https://doi.org/10.1002/art.24984.

[3] A.G. White, H.G. Birnbaum, C. Janagap, S. Buteau, J. Schein, Direct and indirect costs of pain therapy for osteoarthritis in an insured population in the United States, J. Occup. Environ. Med. 50 (2008) 998–1005, https://doi.org/10.1097/JOM.

0b013e3181715111.
[4] C.G. Helmick, D.T. Felson, R.C. Lawrence, S. Gabriel, R. Hirsch, C.K. Kwoh, M.H. Liang, H.M. Kremers, M.D. Mayes, P.A. Merkel, S.R. Pillemer, J.D. Reveille, J.H. Stone, Estimates of the prevalence of arthritis and other rheumatic conditions in the United States. Part I, Arthritis Rheum. 58 (2008) 15–25, https://doi.org/10.1002/art.23177.
[5] D.T. Felson, A. Naimark, J. Anderson, L. Kazis, W. Castelli, R.F. Meenan, The prevalence of knee osteoarthritis in the elderly. The Framingham Osteoarthritis Study, Arthritis Rheum. 30 (1987) 914–918, https://doi.org/10.1002/art.1780300811.
[6] M.C. Hochberg, R.C. Lawrence, D.F. Everett, J. Cornoni-Huntley, Epidemiologic associations of pain in osteoarthritis of the knee: data from the National Health and Nutrition Examination Survey and the National Health and Nutrition Examination-I Epidemiologic Follow-up Survey, Semin. Arthritis Rheum. 18 (1989) 4–9, https://doi.org/10.1016/0049-0172(89)90008-5.
[7] C. Buckland-Wright, Which radiographic techniques should we use for research and clinical practice? Best Pract. Res. Clin. Rheumatol. 20 (2006) 39–55, https://doi.org/10.1016/j.berh.2005.08.002.
[8] G. Jones, C. Ding, F. Scott, M. Glisson, F. Cicuttini, Early radiographic osteoarthritis is associated with substantial changes in cartilage volume and tibial bone surface area in both males and females, Osteoarthr. Cartil. 12 (2004) 169–174, https://doi.org/10.1016/j.joca.2003.08.010.
[9] R.D. Altman, G.E. Gold, Atlas of Individual Radiographic Features in Osteoarthritis, Revised, (2007), https://doi.org/10.1016/j.joca.2006.06.017.
[10] G.W. Stachowiak, M. Wolski, T. Woloszynski, P. Podsiadlo, Detection and prediction of osteoarthritis in knee and hand joints based on the X-ray image analysis, Biosurface and Biotribology 2 (2016) 162–172, https://doi.org/10.1016/j.bsbt.2016.11.004.
[11] K.D. Brandt, R.S. Fife, E.M. Braunstein, B. Katz, Radiographic grading of the severity of knee osteoarthritis: relation of the Kellgren and Lawrence grade to a grade based on joint space narrowing, and correlation with arthroscopic evidence of articular cartilage degeneration, Arthritis Rheum. 34 (1991) 1381–1386, https://doi.org/10.1002/art.v34.
[12] E. Yusuf, M.C. Kortekaas, I. Watt, T.W.J. Huizinga, M. Kloppenburg, Do knee abnormalities visualised on MRI explain knee pain in knee osteoarthritis? A systematic review, Ann. Rheum. Dis. 70 (2011) 60–67, https://doi.org/10.1136/ard.2010.131904.
[13] C. Ding, F. Cicuttini, G. Jones, How important is MRI for detecting early osteoarthritis? Nat. Clin. Pract. Rheumatol. 4 (2008) 4–5, https://doi.org/10.1038/ncprheum0676.
[14] V.B. Kraus, J.E. Collins, H.C. Charles, C.F. Pieper, L. Whitley, E. Losina, M. Nevitt, S. Hoffmann, F. Roemer, A. Guermazi, D.J. Hunter, OA biomarkers consortium, predictive validity of radiographic trabecular bone texture in knee osteoarthritis, Arthritis Rheum. 70 (2018) 80–87, https://doi.org/10.1002/art.40348.
[15] G. Castellano, L. Bonilha, L.M. Li, F. Cendes, Texture analysis of medical images, Clin. Radiol. 59 (2004) 1061–1069, https://doi.org/10.1016/j.crad.2004.07.008.
[16] J.W. Mackay, P.J. Murray, B. Kasmai, G. Johnson, S.T. Donell, A.P. Toms, Subchondral Bone in Osteoarthritis: Association Between Mri Texture Analysis and Histomorphometry, (2017), https://doi.org/10.1016/j.joca.2016.12.011.
[17] J.W. MacKay, G. Kapoor, J.B. Driban, G.H. Lo, T.E. McAlindon, A.P. Toms, A.W. McCaskie, F.J. Gilbert, Association of subchondral bone texture on magnetic resonance imaging with radiographic knee osteoarthritis progression: data from the Osteoarthritis Initiative Bone Ancillary Study, Eur. Radiol. 28 (2018) 4687–4695, https://doi.org/10.1007/s00330-018-5444-9.
[18] E.L. Radin, R. Rose, Role of subchondral bone in the initiation and progression of cartilage damage, Clin. Orthop. Relat. Res. NA (1986) 34–40, https://doi.org/10.1097/00003086-198612000-00005.
[19] H. Weinans, M. Siebelt, R. Agricola, S.M. Botter, T.M. Piscaer, J.H. Waarsing, Pathophysiology of peri-articular bone changes in osteoarthritis, Bone (2012), https://doi.org/10.1016/j.bone.2012.02.002.
[20] H. Imhof, I. Sulzbacher, S. Grampp, C. Czerny, S. Youssefzadeh, F. Kainberger, Subchondral bone and cartilage disease: a rediscovered functional unit, Investig. Radiol. (2000), https://doi.org/10.1097/00004424-200010000-00004.
[21] L. Kamibayashi, U.P. Wyss, T.D.V. Cooke, B. Zee, Trabecular microstructure in the medial condyle of the proximal tibia of patients with knee osteoarthritis, Bone (1995), https://doi.org/10.1016/8756-3282(95)00137-3.
[22] H. Matsui, M. Shimizu, H. Tsuji, Cartilage and subchondral bone interaction in osteoarthrosis of human knee joint: a histological and histomorphometric study, Microsc. Res. Tech. (1997), https://doi.org/10.1002/(SICI)1097-0029(19970515)37:4<333::AID-JEMT8>3.0.CO;2-L.
[23] B.C. Roberts, D. Thewlis, L.B. Solomon, G. Mercer, K.J. Reynolds, E. Perilli, Systematic mapping of the subchondral bone 3D microarchitecture in the human tibial plateau: variations with joint alignment, J. Orthop. Res. 35 (2017) 1927–1941, https://doi.org/10.1002/jor.23474.
[24] A.J. Fields, S.K. Eswaran, M.G. Jekir, T.M. Keaveny, Role of trabecular microarchitecture in whole-vertebral body biomechanical behavior, J. Bone Miner. Res. (2009), https://doi.org/10.1359/jbmr.090317.
[25] P.A. Dieppe, Relationship between symptoms and structural change in osteoarthritis: what are the important targets for therapy? J. Rheumatol. 32 (6) (2005) 1147–1149 http://www.jrheum.org/content/32/6/1147.
[26] S.N. Edd, P. Omoumi, T.P. Andriacchi, B.M. Jolles, J. Favre, Modeling knee osteoarthritis pathophysiology using an integrated joint system (IJS): a systematic review of relationships among cartilage thickness, gait mechanics, and subchondral bone mineral density, Osteoarthr. Cartil. (2018), https://doi.org/10.1016/j.joca.2018.06.017.
[27] A.W. Palmer, R.E. Guldberg, M.E. Levenston, Analysis of cartilage matrix fixed charge density and three-dimensional morphology via contrast-enhanced microcomputed tomography, Proc. Natl. Acad. Sci. 103 (2006) 19255–19260, https://doi.org/10.1073/pnas.0606406103.
[28] M. Siebelt, J. van Tiel, J.H. Waarsing, T.M. Piscaer, M. van Straten, R. Booij, M.L. Dijkshoorn, G.J. Kleinrensink, J.A.N. Verhaar, G.P. Krestin, H. Weinans, E.H.G. Oei, Clinically applied CT arthrography to measure the sulphated glycosaminoglycan content of cartilage, Osteoarthr. Cartil. (2011), https://doi.org/10.1016/j.joca.2011.07.006.
[29] H.T. Kokkonen, J.S. Jurvelin, V. Tiitu, J. Töyräs, Detection of mechanical injury of articular cartilage using contrast enhanced computed tomography, Osteoarthr. Cartil. 19 (2011) 295–301, https://doi.org/10.1016/j.joca.2010.12.012.
[30] D. Mittelstaedt, Y. Xia, Depth-dependent glycosaminoglycan concentration in articular cartilage by quantitative contrast-enhanced micro–computed tomography, Cartilage 6 (2015) 216–225, https://doi.org/10.1177/1947603515596418.
[31] D. Mittelstaedt, D. Kahn, Y. Xia, Topographical and depth-dependent glycosaminoglycan concentration in canine medial tibial cartilage 3 weeks after anterior cruciate ligament transection surgery-a microscopic imaging study, Quant. Imaging Med. Surg. 6 (2016) 648–660, https://doi.org/10.21037/qims.2016.06.12.
[32] L. Xie, A.S.P. Lin, M.E. Levenston, R.E. Guldberg, Quantitative assessment of articular cartilage morphology via EPIC-μCT, Osteoarthr. Cartil. (2009), https://doi.org/10.1016/j.joca.2008.07.015.
[33] L. Xie, A.S.P. Lin, K. Kundu, M.E. Levenston, N. Murthy, R.E. Guldberg, Quantitative imaging of cartilage and bone morphology, reactive oxygen species, and vascularization in a rodent model of osteoarthritis, Arthritis Rheum. 64 (2012) 1899–1908, https://doi.org/10.1002/art.34370.
[34] H.Y. Stevens, B.E. Shockley, N.J. Willett, A.S.P. Lin, Y. Raji, R.E. Guldberg, S.A. Labib, Particulated juvenile articular cartilage implantation in the knee: a 3-year EPIC-μCT and histological examination, Cartilage 5 (2014) 74–77, https://doi.org/10.1177/1947603513515483.
[35] H.J. Yoo, S.H. Hong, J.-Y. Choi, I.J. Lee, S.J. Kim, J.-A. Choi, H.S. Kang, Contrast-enhanced CT of articular cartilage: experimental study for quantification of glycosaminoglycan content in articular cartilage, Radiology 261 (2011) 805–812, https://doi.org/10.1148/radiol.11102495.
[36] J. van Tiel, M. Siebelt, M. Reijman, P.K. Bos, J.H. Waarsing, A.M. Zuurmond, K. Nasserinejad, G.J.V.M. van Osch, J.A.N. Verhaar, G.P. Krestin, H. Weinans, E.H.G. Oei, Quantitative in vivo CT arthrography of the human osteoarthritic knee to estimate cartilage sulphated glycosaminoglycan content: correlation with ex-vivo reference standards, Osteoarthr. Cartil. 24 (2016) 1012–1020, https://doi.org/10.1016/j.joca.2016.01.137.
[37] F.M. Lambers, G. Kuhn, R. Müller, Advances in multimodality molecular imaging of bone structure and function, Bonekey Rep. 1 (2012) 37, , https://doi.org/10.1038/bonekey.2012.28.
[38] J. Schindelin, I. Arganda-Carreras, E. Frise, V. Kaynig, M. Longair, T. Pietzsch, S. Preibisch, C. Rueden, S. Saalfeld, B. Schmid, J.-Y. Tinevez, D.J. White, V. Hartenstein, K. Eliceiri, P. Tomancak, A. Cardona, Fiji: an open-source platform for biological-image analysis, Nat. Methods 9 (2012) 676–682, https://doi.org/10.1038/nmeth.2019.
[39] W.E. Lorensen, H.E. Cline, Marching cubes: a high resolution 3D surface construction algorithm, Proc. 14th Annu. Conf. Comput. Graph. Interact. Tech. - SIGGRAPH '87, 1987, pp. 163–169, , https://doi.org/10.1145/37401.37422.
[40] T. Hildebrand, P. Ruegsegger, A new method for the model-independent assessment of thickness in three-dimensional images, J. Microsc. 185 (1997) 67–75, https://doi.org/10.1046/j.1365-2818.1997.1340694.x.
[41] E. Verhulp, B.va. Rietbergen, R. Huiskes, A three-dimensional digital image correlation technique for strain measurements in microstructures, J. Biomech. 37 (2004) 1313–1320, https://doi.org/10.1016/j.jbiomech.2003.12.036.
[42] R Core team, R Core Team, R A Lang. Environ. Stat. Comput. R Found. Stat. Comput. Vienna, Austria. ISBN 3-900051-07-0, URL Http://Www.R-Project.Org/, 55 (2015), pp. 275–286 http://www.mendeley.com/research/r-language-environment-statistical-computing-96/%5Cnpapers2://publication/uuid/A1207DAB-22D3-4A04-82FB-D4DD5AD57C28.
[43] A. Kroker, J.L. Bhatla, C.A. Emery, S.L. Manske, S.K. Boyd, Subchondral bone microarchitecture in ACL reconstructed knees of young women: a comparison with contralateral and uninjured control knees, Bone 111 (2018) 1–8, https://doi.org/10.1016/j.bone.2018.03.006.
[44] A. Kroker, Y. Zhu, S.L. Manske, R. Barber, N. Mohtadi, S.K. Boyd, Quantitative in vivo assessment of bone microarchitecture in the human knee using HR-pQCT, Bone 97 (2017) 43–48, https://doi.org/10.1016/j.bone.2016.12.015.
[45] H.J. Nieminen, H.K. Gahunia, K.P.H. Pritzker, T. Ylitalo, L. Rieppo, S.S. Karhula, P. Lehenkari, E. Hæggström, S. Saarakkala, 3D histopathological grading of osteochondral tissue using contrast-enhanced micro-computed tomography, Osteoarthr. Cartil. 25 (2017) 1680–1689, https://doi.org/10.1016/J.JOCA.2017.05.021.
[46] J.L. Bhatla, A. Kroker, S.L. Manske, C.A. Emery, S.K. Boyd, Differences in subchondral bone plate and cartilage thickness between women with anterior cruciate ligament reconstructions and uninjured controls, Osteoarthr. Cartil. (2018), https://doi.org/10.1016/j.joca.2018.04.006.
[47] A. Kroker, S.L. Manske, N. Mohtadi, S.K. Boyd, A study of the relationship between meniscal injury and bone microarchitecture in ACL reconstructed knees, Knee (2018), https://doi.org/10.1016/j.knee.2018.07.004.
[48] P. Omoumi, N. Michoux, E. Thienpont, F.W. Roemer, B.C. Vande Berg, Anatomical distribution of areas of preserved cartilage in advanced femorotibial osteoarthritis using CT arthrography (part 1), Osteoarthr. Cartil. 23 (2015) 83–87, https://doi.org/10.1016/J.JOCA.2014.10.006.